Title: Selected physico-chemical properties of composite scaffolds of sintered submicrocrystalline corundum and bioglass

Author: Barbara Staniewicz-Brudnik, Małgorzata Karolus, Katarzyna Cholewa-Kowalska, Grzegorz Skrabalak, Jolanta Laszkiewicz-Łukasik, Justyna Drukała, Joanna Stalińska, Katarzyna Dziedzic

Citation style: Staniewicz-Brudnik Barbara, Karolus Małgorzata, Cholewa-Kowalska Katarzyna, Skrabalak Grzegorz, Laszkiewicz-Łukasik Jolanta, Drukała Justyna, Stalińska Joanna, Dziedzic Katarzyna. (2022). Selected physico-chemical properties of composite scaffolds of sintered submicrocrystalline corundum and bioglass. „ The International Journal of Advanced Manufacturing Technology” (16 Feb 2022), DOI: 10.1007/s00170-022-08736-w

The International Journal of Advanced Manufacturing Technology
https://doi.org/10.1007/s00170-022-08736-w

ORIGINAL ARTICLE

Selected physico-chemical properties of composite scaffolds of sintered submicrocrystalline corundum and bioglass

Barbara Staniewicz-Brudnik[1] · Małgorzata Karolus[2] · Katarzyna Cholewa-Kowalska[3] · Grzegorz Skrabalak[1] · Jolanta Laszkiewicz-Łukasik[1] · Justyna Drukała[4] · Joanna Stalińska[4] · Katarzyna Dziedzic[4]

Received: 26 August 2021 / Accepted: 13 January 2022

Abstract

Presented paper contains description and interpretation of the results of selected physicochemical and structural properties of two types of composite sinters. They were constituted of a mixture of sintered microcrystalline corundum and bioglass CaO-P_2O_5-SiO_2-Na_2O system intended for scaffolds to cell culture of human chondrocytes. The composites contained a mixture of both above-mentioned components in the volumetric proportion of 50:50 (W5) and 30:70 (W7). They were obtained using powder metallurgy by free sintering in air atmosphere. Phase analysis of composites and verification of theoretical identification using X-ray diffraction were performed. The same phases were found in both cases (Al_2O_3 SiO_2 $CaAl_2Si_2O_8$, $Ca_3(PO_4)_2$, $Ca_2Al_4O_7$ and $NaAlSiO_4$). Microscopic tests of composite surfaces were performed and some differences were found. W5 sample was not completely covered with bioglass, whilst W7 sample was completely covered with bioglass with few fine pores. Tests of surface topography confirmed the presence of large and small pores. Composite surfaces immersed for 30 days in artificial blood plasma were tested and then electron microscopy analysis was performed. It was found that no significant changes occurred on the surface of the W5 composite, probably partial corrosion of the glass happened. Spherical forms characteristic of HA-hydroxyapatites were observed on the surface of sample W7. Human articular chondrocyte cells were seeded on both types of sinters and proliferation assay was performed. Results indicate that tested scaffolds support cellular attachment and proliferation of chondrocytes.

Keywords Submicrocrystalline sintered corundum · Bioglass · Scaffolds · SEM · XRD · SBF · Surface topography

1 Introduction

The dynamic development of biomaterial engineering, the search for new biocompatible substances and materials that can replace damaged tissues and organs have caused a change in the proportion of biomaterials (metals and metal alloys, polymers and inorganic composites) towards composite materials over the past two decades. The demand for biomaterials results mostly from the growing number of communication injuries, injuries resulting from practicing sports, including extreme sports and development of civilization diseases. It is also associated with progress in the development of various fields of reconstructive surgery, interventional surgery and prosthetics [1–4]. One of the most interesting biocomposites used in bone regenerative medicine comes in the form of corundum ceramic composites modified with various additives (bioglass polymers) obtained by different techniques. Most researchers studying corundum implants and their use in modern bone surgery claim that

Highlights
- Scaffolds composites, structure identification by VCS algorithm and XRD diffraction, surface topography of scaffolds, SBF test, proliferation test of chondrocyte.

✉ Małgorzata Karolus
karolus@us.edu.pl

[1] Centre of Manufacturing Technology- Łukasiewicz Research Network, Krakow Institute of Technology, Zakopiańska 77, 30-418 Kraków, Poland

[2] Institute of Materials Engineering, University of Silesia, 75 Pułku Piechoty 1a, 41-500 Chorzów, Poland

[3] AGH University of Science and Technology, Al. Mickiewicza 30, 30-059 Kraków, Poland

[4] Department of Cell Biology, Faculty of Biochemistry, Biophysics and Biotechnology, Jagiellonian University, Gronostajowa 7, 30-387 Kraków, Poland

Published online: 16 February 2022

corundum material does not produce strong chemical connection with bone tissue. The addition of corundum bioglass from the CaO-P_2O_5-SiO_2-Na_2O system into the corundum matrix affects mostly the possibility of creating chemical bonding with bone tissue. Modifying the composite with bioglass results in obtaining new strength characteristics, which also affects surface properties that appear to cause increased cell proliferation. Corundum ceramic composites modified with bio-glasses are characterized by [5–8]:

- Porosity that enables tissue ingrowth, securing permanent connection between tissue and implant
- High biocompatibility and bioactivity in the tissue environment
- High compressive strength and abrasion resistance
- Possibility of sterilisation without changing the properties of materials
- Easy shaping of the material by conventional means

Currently, ceramic composites containing bioglass and glass–ceramics are already used not only as experimental material but also in clinical practice [5, 9, 10] as:

- Middle ear implants (solid MEP® and Douek-MED™ fittings—Bioglass® 45S5 Cervital®)
- Restoration after tooth extraction (solid REMI® – Bioglass 45S5 shapes)
- Filling of bone defects (powder or granules: PerioGlas® Biogran®—Bioglass® 45S5; powder and granules: BinAlive-glass S53P4; granules: Cerabone®)
- Implants and fillings in craniofacial surgery (NoveBone® lite powder, Ilmaplant® shapes)
- Porous scaffolds for tissue engineering
- Drug delivery system

The aim of the research and their innovation was the use of a non-toxic abrasive material sintered submicrocrystalline corundum with an active bioglass from the CaO-P_2O_5-SiO_2-Na_2O system to obtain a biocomposite. Developed material is intended to be used for the cultivation of human chondrocyte cells (W5, W7). The program of testing biocomposites with different weight content of submicrocrystalline sintered corundum and bioglass (w5, w7) and their results were presented below.

2 Subject matter and methodology

After preliminary analysis of ten biocomposites, two were finally selected for further research [11, 12]. The two kinds of biocomposites (W5, W7) containing submicrocrystalline sintered corundum and bioglass from CaO-SiO_2-P_2O_5-Na_2O system with various proportion of the components (W5-50%vol of glass, W7 70%vol of glass) respectively.

Physical and mechanical properties (microscopic observation, porosity, absorbability, HRB hardness) were tested on 16 × 5 mm and 10 × 2 mm tablets obtained by cold pressing under 75 MPa pressure and freely sintered in an electric furnace. Each of the tests of selected physicochemical properties (porosity, water absorption, hardness) were carried out for five samples of biocomposites W5 and W7. The open porosity was measured with Archimedes method. Previously dried samples are weighted. There are also weighted the apparent mass of the sample saturated with liquid in a vacuum and the apparent mass of the sample saturated with liquid in the air. Porosity is defined as the ratio of the total open pore volume to its apparent volume. The water absorption was determined by the hydrostatic method based on the formula (1):

$$N = [(m_2 - m_1)/m_1] \times 100\% \quad (1)$$

where:

$N\Delta$ Absorbability
m_1 Mass of dried sample
m_2 Mass of sample after immersion in water

The heat treatment process was carried out according to predetermined characteristics with stabilisation for two hours at maximum temperature (770 °C).

Chemical stability calculations at the maximum temperature (750 °C, 770 °C) were carried out using the VCS algorithm. Verification of the obtained results was performed using Empyrean Diffractometer with Cu radiation fully confirming the presence of the calculated compounds. Microscopic observations on the Joel JSM6460 LV scanning electron microscope were made in high vacuum (10^{-5} Torr) at an accelerating voltage of 20 kV, magnification 40 × and 100 × using the BEC image. The geometric structure of the surface was determined using the TOPO01vP profilometer through the measurements of surface topography parameters (R_a, R_z, R_t) and 2D and 3D spatial images.

The hardness of bio composites was determined by reading the values of 1/6 inch steel ball res-cess on the HRB scale on the Rockwell hardness tester. Biocompatibility of the composites was determined by SBF test (immersion of composite samples in artificial blood plasma for 30 days). The surface of composites after a long-term bath on a scanning microscope BEC image was observed and the phase composition of the surface of composites was also analysed. Normal human articular chondrocytes (Lonza) c were seeded on the obtained tablets (as growth substrate) using standard procedure (Chondrocyte Growth Medium, Lonza, 37 °C in 5% CO_2 atmosphere, initial cell density 1×10^4 cells/cm^2) and WST-1 proliferation assay was performed (reading after 72 h, 96 h, 144 h).

2.1 Some physical I mechanical properties of raw and sintered materials

The raw materials used in sintering process were: submicrocrystalline sintered corundum of F 320 (49–16.5 um) and glass from CaO-P_2O_5 SiO_2-Na_2O system marked as FB1 with grain size of about 40 µm. Submicrocrystalline sintered corundum grain is new generation of alfa type aluminium oxide with ultradispersive structure. It might be obtained by transformation of sol–gel process of aluminium oxide by using MgO, L_2O_3 Nd_2O_3 Y_2O_3 as modifiers. Abrasive grains consist of Al_20_3 plates about 0.5–1 µm joint by needle bridge of $MgLaAl_{11}O_{19}$ spinel type. In comparison to conventional corundum materials submicrocrystalline sintered corundum grains have higher strength (90 MPa, conventional 80 MPa), hardness (20–22 GPa, conventional18.5–20 GPa) with simultaneously increase of fracture toughness. Commercial names of these materials are cubitron, Seeded Gel and Blue Sapphire [13].

FB1 glass obtained from CaO-SiO_2-P_2O_5-Na_2O was melted at 1350 °C in electric furnace in air atmosphere and then fritted (poured into cold water). Obtained material belongs to the group of lightweight materials, as its density is of Material has 2.622 g/cm^3. Materials belong to medium hard glasses about4.9 MPa, which have good wettability to cubitron substrate (contact angle $\theta < 30°$ at 850 °C).

The sinters (W5 and W7 selected from ten among previously tested) were obtained by powder metallurgy technique through free sinters in electric furnace in air atmosphere. Their physical and mechanical properties differ significantly (Table 1).

Increasing the glass content caused a decrease in the density of the composite and a significant decrease in open porosity [14].

2.2 Calculation of chemical equilibrium of biocomposites using VCS algorithm

The chemical stability of the sample of the submicrocrystalline sintered corundum–glass of CaO-P_2O_5-SiO_2-Na_2O system was determined by calculating the thermodynamic potential ΔG of the reactions likely to occur between them. The calculations were performed using the VCS algorithm (Villers, Cruise and Smith), taking into account the chemical stability of all probable reaction products.

Equilibrium calculations were done with the method of minimizing the thermodynamic potential of the entire mixture. The mass balance of elements and non-negativity of the mole numbers of individual components was maintained. In this method, the equilibrium composition means a non-negative set of moles of individual components for which the thermodynamic potential ΔG of the entire mixture reaches a minimum whilst meeting the mass balance equations of all elements of the mixture. The formula used was (2):

$$\Delta G = \sum_{i=1}^{N} n_i \mu_i \tag{2}$$

ΔG	thermodynamic potential
n_i	Mnumber of moles of components i
μ_i	chemical potential of components i
N	number of components

Equilibrium calculations with the minimizing thermodynamic potential method did not require any specifying number and form of reactions through which the system reached equilibrium. Specification of the substances that may or may not be in balance was necessary. The premise of the method is that all connections possible from the elements included in the mixture in the equilibrium state could have occurred. The calculations showed that 7 compounds from 100 available mixtures make it possible to create solid state connections. The calculations took into account the number of gram-atoms of glass components and sintered microcrystalline corundum in specific volumes.

For W7, the number of gram-atoms of bioglass components in the volume of 700 cm^3 and the number of gram-atoms of submicrocrystalline corundum sintered in 300 cm^3 of composite were calculated.

For W5, the number of gram-atoms of bioglass components in the volume of 500 cm^3 and the number of gram-atoms of submicrocrystalline corundum sintered in 500 cm^3 of composite were calculated.

The assumption was made that the components of biocomposites in these temperature ranges (750 °C and 770 °C) could have occurred: in the multi-component gas phase, pure condensed phases (liquid and solid), and the liquid phase in which the components were mixed unrestrictedly.

Assumption I: the resulting equilibrium mixture consisted of a multi-component gas phase and pure condensed phases (solid and liquid) that do not mix.

Assumption II: the resulting equilibrium mixture consists of a multi-component gas phase, a multi-component liquid phase, and pure solid phases.

Table 1 Chosen properties of tested materials W5 and W7 samples

Compositions variants	Composite density (g/cm^3)	Theoretical porosity (%)	Open porosity tested (%)	Absorbability tested (%)	Hardness (HRB)
W5	3.328 ± 0.008	21.5 ± 0.1	20.35 ± 0. 3	8.4 ± 0.1	78 ± 2
W7	2.850 ± 0.009	2.1 ± 0.02	1.25 ± 0.01	0.5 ± 0.04	60 ± 1

The equilibrium composition in the number of moles is the same for both these assumptions (Table 2).

Tables 3 and 4 show the compositions of equilibrium systems of W5 and W7 biocomposites at 750 °C, 770 °C for condensed phases.

Verification of the obtained results was performed by use of XRD–phase analyses

2.3 XRD analyses of W5, W7 bio composites

The X-ray experiment was performed with the PANalytical Empyrean Diffractometer with Cu radiation. Phase analysis basing on ICDD PDF 4 + 2017 data base confirmed the presence of Al_2O_3, SiO_2, $CaAl_2Si_2O_8$, $Ca_3(PO_4)_2$, $Ca_2Al_4O_7$, $NaAlSiO_4$ phases. The X-ray diffraction patterns are presented on the Figs. 1 and 2. The detailed structural characteristic of tested W5 and W7 samples are presented in Tables 5 and 6.

The determination of unit cell parameters (a, b, c [Å]), crystallite sizes (D [Å]) and lattice strain (ε [%]) values as well as qualitative phase analysis (amount of phases [wt. %]), presented in the Tables 5 and 6, were refined by using the PANalytical software High Score Plus basing on the Rietveld method [15, 16]. The detailed scheme description of analyses and conditions were presented, among others in [17, 18]. The determination of the crystallite size and the lattice strains were performed basing on the Williamson-Hall method [19]. The patternless quantitative phase analysis is basing on the crystallographic data of analysed materials (unit cell parameters, phase group, atoms positions, absorption coefficients, etc.) [15]. Agreement factors for refinement are comparable to values typical for microcrystalline materials [16] and they are in a range of 7–9%.

In comparison to the theoretical unit cell values (ICDD PDF + 4 2017 data base) of identified phases, the unit cell parameters were slightly changed. The material tested showed the presence of nanocrystalline phases, of the components of the final material from 100 to 450 Å. Only the size of corundum crystallites is in the order of 750–1000 Å. The results of the quantitative phase analysis obtained for samples W5 and W7 show some similarity. However, the amount of Al_2O_3 phase is reduced by about 16% and is respectively 42 wt.% for W5 and 35 wt.% for W7. Also, the amount of SiO_2 phase decreases and is correspondingly 10 wt.% for W5 and 6 wt.% for W7. For the $CaAl_2Si_2O_8$ and $CaAl_4O_7$ phases, a slight increase in the mass amount of components (by 2–3%) in the sample W7 compared to the sample W5 is observed. The mass amount of the remaining phases does not change.

Table 2 VCS algorithm calculation conditions

T [K]	1023.15	1043.15
t [°C]	750	770
P [atm]	1.00	1.00

Table 3 Stable solid compounds according to Assumptions I and II for W5 sample

Variant W5	Assumption I		Assumption II	
Phase composition	750 °C	770 °C	750 °C	770 °C
Al_2O_3	14.200	14.200	14.200	14.200
SiO_2	3.100	3.100	3.100	3.100
$CaAl_2Si_2O_8$	1.345	1.345	1.345	1.345
$Ca_3(PO_4)_2$	0.250	0.250	0.170	0.170
$Ca_2Al_4O_7$	1.119	1.119	1.119	1.119
$NaAlSiO_4$	0.521	0.521	0.521	0.521

2.4 Microscopic observations

Microscopic observations of the W5 and W7 bio composites on a scanning electron microscope (SEM, BEC image) showed, in the case of the W5 sample, uneven coating of glass sintered over submicrocrystalline corundum grains, particularly visible at the grain boundaries. Few deep pores appeared on the surface. The surface of the W7 bio composite sample was evenly covered with glass (Fig. 3) with only a few small pores, which was confirmed by studies of the surfaces.

2.5 Topography of composite surfaces

The measurement of the geometric surface of the W5 and W7 samples showed clear differences in the surface topography by R_a parameters (height of the highest profile rise inside the elementary segment W5 11.764 µm, W7 11.390 µm), R_z (sum of height of the highest rise and largest indentation in the elementary section W5 34.04 µm, W7 44.04 µm and R_t (sum of height of the highest rise and largest indentation of the measured section W5 46.283 µm, W7 66.434 µm). This confirmed the impact of the glass content on the origination

Table 4 Stable solid compounds according to Assumptions I and II for W7 sample

Variant W7	Assumption I		Assumption II	
Phase composition	750 °C	770 °C	750 °C	770 °C
Al_2O_3	11.900	11.900	11.900	11.900
SiO_2	4.020	4.020	4.020	4.020
$CaAl_2Si_2O_8$	1.520	1.520	1.520	1.520
$Ca_3(PO_4)_2$	0.400	0.400	0.320	0.320
$Ca_2Al_4O_7$	1.321	1.321	1.321	1.321
$NaAlSiO_4$	0.645	0.645	0.645	0.645

Table 5 Structural analysis of W5-sample

Phase	Space Group	Amount [wt. %]	*a* [Å]	*b* [Å]	*c* [Å]	*D* [Å]	ε [%]
Al_2O_3	R-3c	42	4.7587(7)	–	12.9926(5)	> 1000	0.075
SiO_2	$P3_22_1$	10	4.9212(2)	–	5.4104(1)	456	0.072
$CaAl_2Si_2O_8$	P-1	9	8.1591(7)	12.6111(6)	12.9240(8)	364	0.421
$CaAl_4O_7$	C2/c	25	13.0595(1)	9.1355(1)	5.4668(6)	73	0.447
$NaAlSiO_4$	$P6_3$	10	9.9806(8)	–	8.2909(7)	232	0.140
$Ca_3(PO_4)_2$	$P2_1/c$	4	5.0088(5)	18.2004(9)	–	275	0.119

of fine deep pores on composite surface. Together with the increasing content of bioglass in the composite, the increase in the number of small-width pores was observed. Symmetrical system was found in the analysis of the material share graph of the W5 sample (Fig. 4a), without characteristic, random extreme surface elements (rises and indentations). In case of the W7 sample, the material share graph showed an upward shift, which proved occurrence of individual narrow, deep cavities (Fig. 5a).

2.6 Bioactivity assessment—SBF test

Samples of W5 and W7 composite scaffolds were prepared for the SBF test by heating in an electric oven at 300 °C for 1 h, washing with 96% ethanol and steam sterilising in an autoclave at 120 °C. The samples were immersed in an artificial blood plasma (SBF) solution that was previously filtered with a 0.22 µm syringe filter. After 30 days of the samples incubation, pH of the SBF solution was slightly higher than initial and equal to 7.61 (initial 7.4) due to Na^+ and Ca^{2+} release from glass as a composite component. The SEM/EDX analysis after the final incubation period showed no significant surface changes for W5 sample, with only larger pores occurring. It was most likely that the $Na^+/Ca2^+$ ions from glass were exchanged for H^+ ions from SBF solution resulted in a layer rich in Si (a layer of silica gel). However, no crystallization of calcium phosphates was observed, which might probable be associated with a positive surface charge due to a high content of Al_2O_3. According to the literature, point of zero charge for alumina is around pH 8.5–9.0, so we expected that at pH close to 7.4 the composite surface has a positive charge and thus Ca^{2+} and phosphate ions chemisorption and subsequently HA formation may be hindered [20]. Specifically, positively charged surface has an affinity for phosphate ions adsorption but it shown only a slight attraction towards calcium ions at this pH [21]. Due to the formation of stable surface alumina-phosphate complexes with a very low tendency toward calcium adsorption, the lack of calcium phosphate formation is observed.

The entire surface of the W7 sample presented fine spherical forms with morphology characteristic of HA-hydroxyapatite. EDX analysis showed that only P and Ca were present on the surface, the lack of Si and Al in surface composition may suggest that the formed layer is thicker than 1 µm. The Ca/P ratio was 1.55, which proved the formation of HA with Ca deficit. The presence of Na^+ and Mg^{2+} ions in the surface layer composition most likely means the share of these elements in the structure of forming HA as a substitution in the cationic subnet. At this case, the surface had negative charge due to higher (70%) bioactive glass content, and silanols groups (Si–OH formed during SBF incubation) act as nucleating sites for the calcium phosphate formation. Regarding to the pH, after 30 days immersion of composites, the pH of the SBF was very similar mainly due to the limited solubility of ions from W5 composites and in turn chemisorption of ions from SBF in the case of W7 material. These results reveal that the W7 composites show bioactive properties, whilst W5 materials are only biocompatible.

2.7 Culture of human articular chondrocytes on biocomposite scaffolds

Preparation of biocomposite scaffolds for seeding of human chondrocyte cells consisted of sterilisation by

Table 6 Structural analysis of W7-sample

Phase	Space Group	Amount [wt. %]	*a* [Å]	*b* [Å]	*c* [Å]	*D* [Å]	ε [%]
Al_2O_3	R-3c	35	4.7574(4)	–	12.9936(2)	730	0.045
SiO_2	$P3_22_1$	6	4.9527(7)	–	5.2503(2)	129	0.253
$CaAl_2Si_2O_8$	P-1	14	8.1355(2)	12.8189(9)	12.6271(1)	323	0.101
$CaAl_4O_7$	C2/c	31	12.8378(2)	9.1979(5)	5.3604(8)	123	0.266
$NaAlSiO_4$	$P6_3$	10	9.9386(2)	–	8.3157(8)	286	0.114
$Ca_3(PO_4)_2$	$P2_1/c$	4	4.7632(9)	18.8053(1)	–	491	0.067

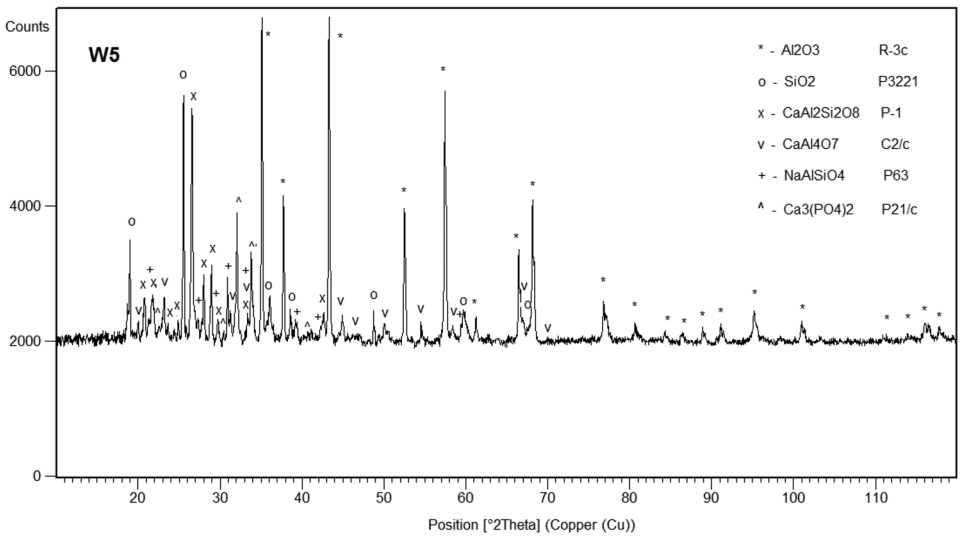

Fig. 1 X-ray diffraction pattern of W5 samples

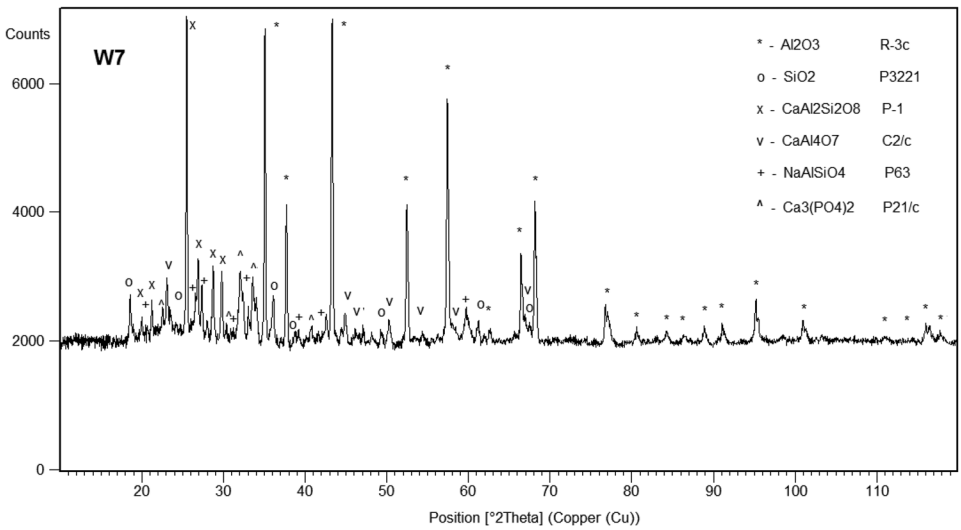

Fig. 2 X-ray diffraction pattern of W7-sample sample

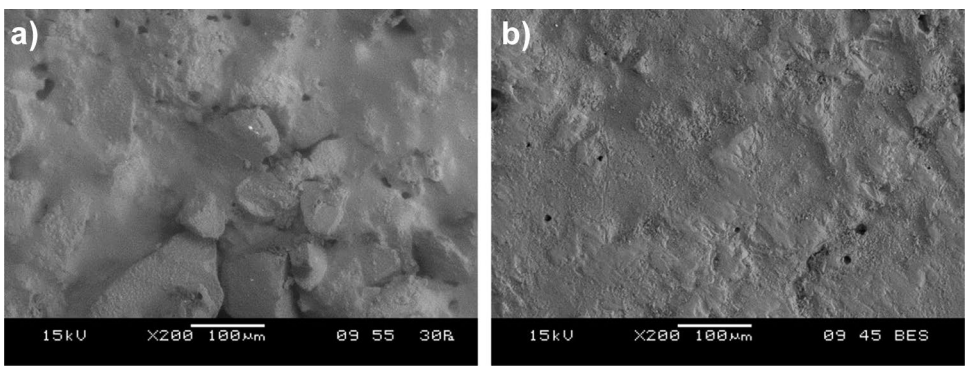

Fig. 3 SEM micrograph of the surface of W5 (**a**) and W7 (**b**) samples at 200 × magnification

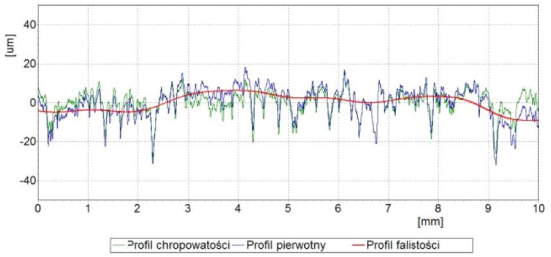

a)

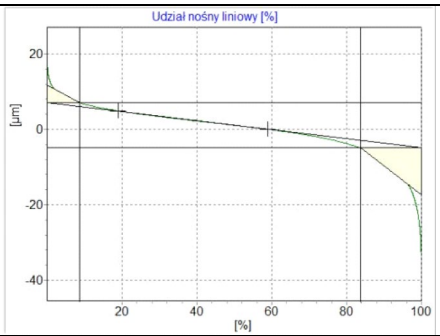

b)

	Avg	S	Min	Max	Spacing
Ra [µm]	4.644	0.511	3.510	6.101	2.592
Rq [µm]	6.237	0.707	4.724	8.467	3.743
Rp [µm]	11.764	1.319	9.033	16.714	7.680
Rv [µm]	22.642	3.039	15.507	31.115	15.608
Rz [µm]	34.406	3.592	26.089	44.220	18.131
Rc [µm]	11.346	1.519	8.033	15.561	7.528
Rt [µm]	46.283	5.903	31.574	63.822	32.248

c)

d)

Fig. 4 Topography of the W5 sample surface: roughness profile (**a**), linear load share (**b**), horizontal parameter values (**c**), and surface map (**d**)

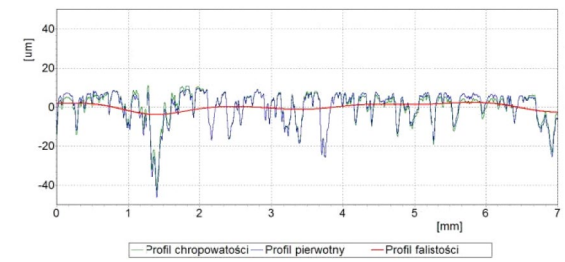

a)

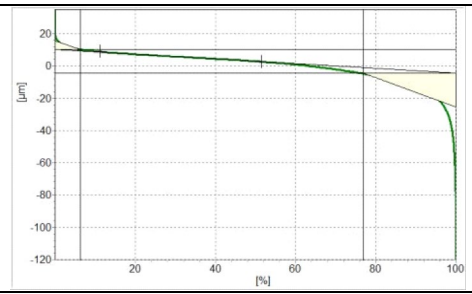

b)

	Avg	S	Min	Max	Spacing
Ra [µm]	7.459	1.423	4.463	11.807	7.344
Rq [µm]	9.845	2.274	5.899	17.651	11.752
Rp [µm]	11.390	2.159	6.829	19.787	12.958
Rv [µm]	33.295	8.849	19.800	64.965	45.165
Rz [µm]	44.685	10.542	26.805	80.696	53.891
Rc [µm]	18.611	4.324	11.937	47.025	35.088
Rt [µm]	68.434	22.656	34.939	141.764	106.825

c)

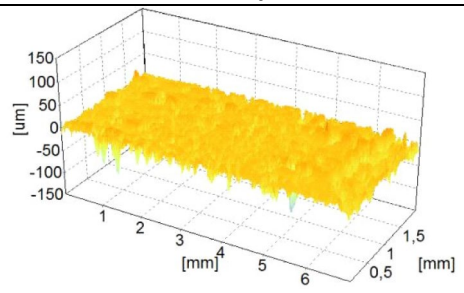

d)

Fig. 5 Topography of the W7 sample surface: roughness profile (**a**), linear load share (**b**), horizontal parameter values (**c**), and surface map (**d**)

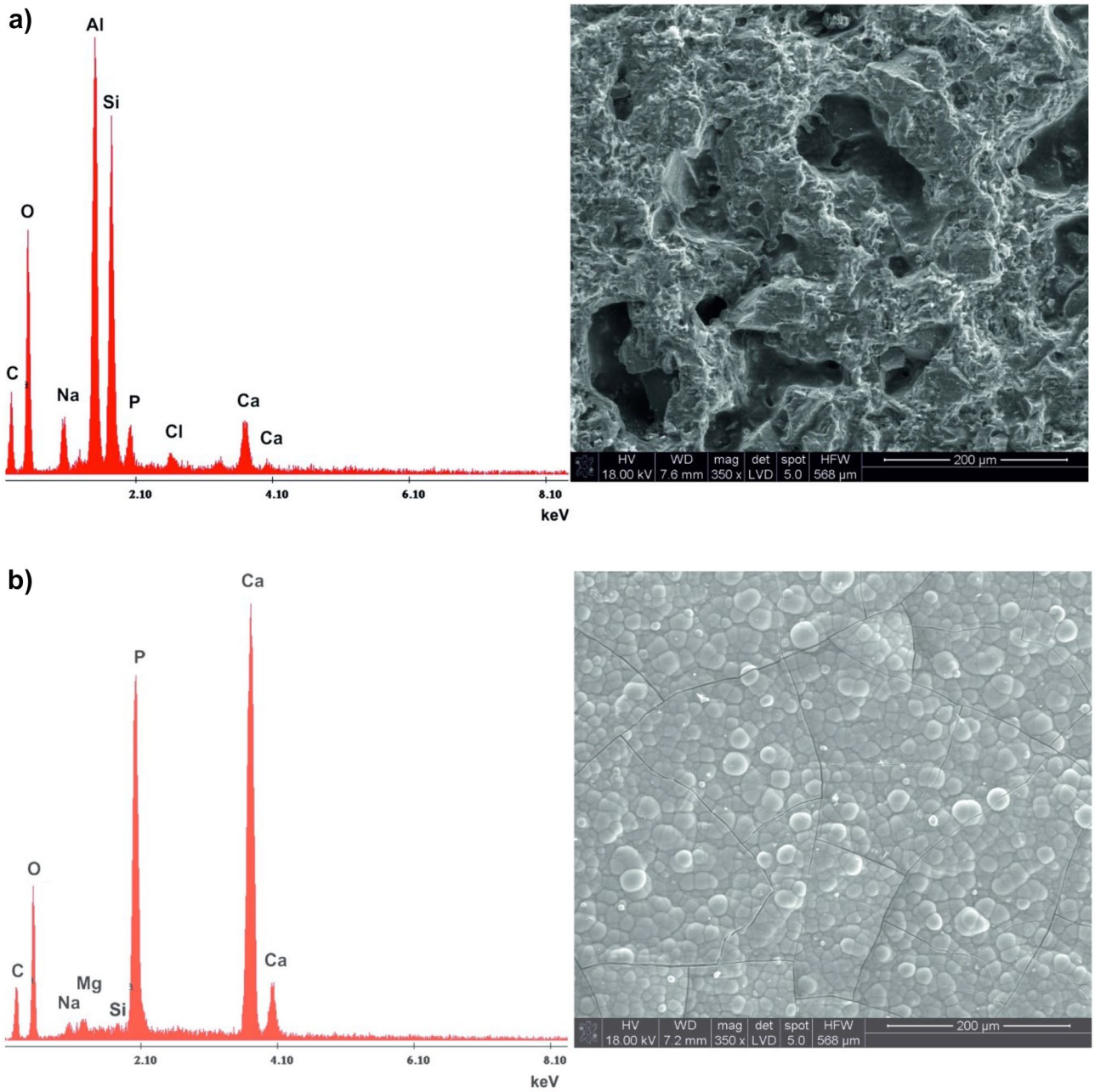

Fig. 6 **a** Microphotographs of SEM and EDS diagram of W5 sample after 30 days incubation in SBF. **b** Microphotographs of SEM and EDS diagram of W7sample after 30 days incubation in SBF.

24 h incubation with 70% Et0H and UV lamp irradiation for 40 min on each side. The proliferation assay was performed using the Cell proliferation reagent WST-1 kit (Roche Diagnostics) based on the measurement of cell metabolic activity. As the number of cultured cells increases, the amount of mitochondrial dehydrogenase enzymes increases, which convert the tetrazolium salt WST-1 into a coloured product. Normal human articular chondrocytes (NHAC-kn, Lonza, passage 4–5) were seeded on the tablets at an initial density of 1×10^{4}cell/cm^2, with tissue-culture treated polystyrene serving as the control substrate for the growth of the cells. WST-1 assay was performed at the end of a 72, 96 or 144-h incubation, according to the manufacturer's instructions. A plot of the time dependence of the absorbance values for the composites tested (W5, W7) is shown below. It was found that the chondrocytes adhered to the scaffolds and the tested substrates allowed for cell proliferation. However, the proliferation rate was lower than under control conditions and no significant differences were observed in proliferation

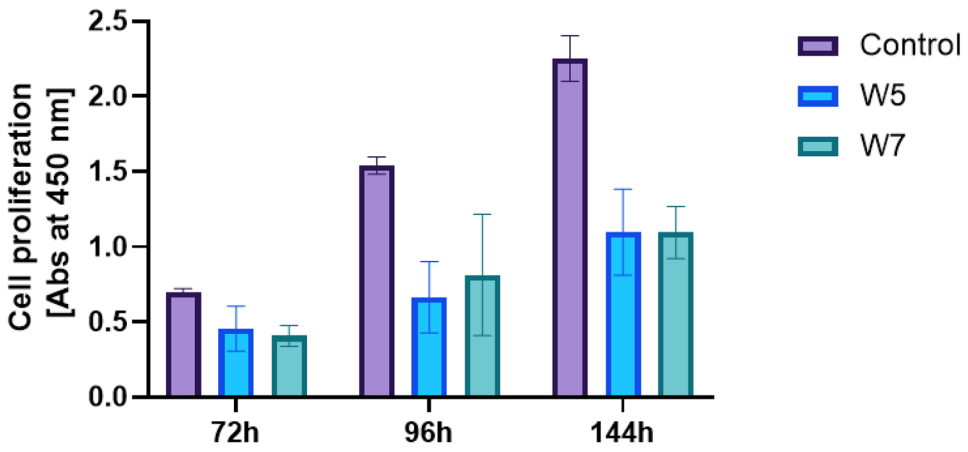

Fig. 7 WST-1 cell proliferation assay (absorbance was measured at 450 nm). Normal human articular chondrocytes were plated on the scaffolds and incubated for 72, 96 or 144 h. Cells plated on tissue-culture treated polystyrene served as a control. Data represent mean values ± SD

between w5 and w7 scaffolds. Lower rates of cell proliferation can, however, be associated with maintaining the desirable phenotype of articular chondrocytes and it may prevent the de-differentiation of chondrocytes in in vitro cell culture (Fig. 6).

Experiments were performed twice in triplicate for each experimental condition. Data represent mean values ± SD. Statistical analysis was performed using GraphPad Prism8.0 (Fig. 7).

3 Conclusions

The following concludes the studies of W5 and W7 composite scaffolds with submicrocrystalline sintered corundum and FB1 bioglass:

- Increasing the FB1 glass content (from 50 to 70% by volume) significantly affected open porosity of sinters and their absorptivity (W5: porosity 20%, absorptivity 8.4%; W7: porosity 1.25%, absorptivity 0.5%)
- VCS calculations verified by X-ray tests showed the presence of Al_2O_3, SiO_2, $CaAl_2Si_2O_8$, $CaAl_4O_7$, $NaAlSiO_4$ and $Ca_3(PO_4)_2$ in both composites
- Microscopic image (SEM, BEC) of W5 scaffold composites showed incomplete FB1 glass coverage of sintered microcrystalline corundum grains and visible large pores between corundum grains (Fig. 6). The W7 composite surface, however, was evenly covered with glass with narrow, fine pores
- Measurements of the geometric surface of scaffolds W5 and W7 showed clear differences in the parameters: R_p (W5—11.764 µm, W7—11.390 µm), R_z (W5—34.04 µm, W7—44.04 µm) and R_t (W5—46.283 µm, W7—66.434 µm). The graph of W7 sinter material showed upward shift, which indicated the presence of narrow, deep cavities
- The SEM/EDX analysis after the final incubation period showed no significant surface changes for W5 sample, with only larger pores occurring. It was most likely that the $Na^+/Ca2^+$ ions from glass were exchanged for H^+ ions from SBF solution resulted in a layer rich in Si (a layer of silica gel) The W7 sinter surface, however, was covered with spherical forms characteristic of HA-hydroxyapatite. EDX analysis confirmed the presence of only Ca and P in a ratio of Ca/P 1.55, which indicated the formation of HA with Ca deficiency
- Both substrates (W5 and W7) were biocompatible despite differences in SBF assay behaviour, as confirmed by the WST-1 assay. The substrates tested allowed for the proliferation of human chondrocytes (increase in absorbance in the WST-1 assay with increasing incubation time); however, the proliferation rate was lower than in the reference conditions (tissue culture plastic). No significant differences in cell proliferation were observed between the tested substrates.

Acknowledgements The project was carried out with the Łukasiewicz—Krakow Institute of Technology own founds.

Author contribution Conceptualization, B.S.-B.; methodology, B.S.-B., J.D., and M.K.; validation, B.S.-B., M.K.; formal analysis: B.S.-B., J.D., J.L.-Ł.,K.C.-K., J.S., K.S., G.S., and M.K.; investigation, B.S.-B., J.D., J.L.-Ł.,K.C.-K., J.S., K.S., G.S., and M.K.; resources, B.S.-B.; M.K., data curation, B.S.-B.; writing—original draft preparation, B.S.-B.; writing—review and editing, B.S.-B.; visualization, B.S.-B., G.S., and M.K.; supervision, B.S.-B.; project administration, B.S.-B.; funding acquisition, B.S.-B.

Funding The project was carried out at Łukasiewicz–IAMT own funds.

Data availability Not applicable.

Code availability Not applicable.

Declarations

Ethics approval There is no research involving Human Participants and Animals.

Conflict of interest The authors declare no conflict of interest.

References

1. Błażewicz S, Stoch L (2003) Akademicka Oficyna Wydawnicza Exit, Warszawa. Biomaterials 4 (in Polish)
2. Świeczko-Żurek B (2009) Biomaterials WPG (in Polish)
3. Boccaccini AR, Gerhardt LC (2010) Bioactive glass and glass-ceramic scaffolds for bone tissue engineering (ed.). Materials 3:2867–3910
4. Ratner BD, Hoffman AS, Schoen FJ, Lemons JE (1996) Biomaterials Science: An introduction to materials in medicine (ed). Academic Press
5. Dziadek M, Pawlik J, Cholewa-Kowalska K (2014) Bioactive glasses for tissue engineering. Acta Bio-Optica et Informatica Medica. Inżynieria Biomedyczna 20(3):156–165 (in Polish)
6. Dziadek M, Zagrajczuk B, Jeleń P, Olejniczak Z, Cholewa-Kowalska K (2016) Structural variations of bioactive glasses obtained by different synthesis routes. Ceram Int 42(13):14700–14709
7. Sachlos E, Czernuszka JT (2003) Making tissue engineering scaffolds work. Review on the application of solid freeform fabrication technology to the production of tissue engineering scaffolds. AO Research Institute Davos, Davos. Eur Cells Mater
8. Staniewicz-Brudnik B, Lekka M (2012) Biocompatible glass-ceramic composite- manufacturing and selected physicalmechanical properties. Sintering of Ceramics, new Emerging Techniques / Book. ISBN 978–953–51–0017–1. Ed: Prof. Dr Arunachalam Lakshmanan. Saveetha Engineering College, Thandalam, Chennai, India, chapter 11 pp 227–250
9. Yang F, Li C, Lin Y, Wang CA (2012) Effects of sintering temperature on properties of porous mullite/corundum ceramics. Mater Lett 73:36–39
10. Jaegermann Z, Ślósarczyk A (2007) Dense and porous corundum bioceramics in medical application Uczelniane Wydawnictwo Naukowo–Dydaktyczne AGH, Kraków (in Polish)
11. Staniewicz-Brudnik B, Lekka M, Bączek E, Wodnicka K, Miller T, Wilk W (2012) Biocomposites with submicrocrystalline sintered corundum and bioglass system as a scaffolds and their structural and physical properties. Short and long-term culture of the fibroblast human skin on these substrate. Optica Applicata 42(2):387–397
12. Staniewicz-Brudnik B, Lekka M, Jaworska L, Wilk W (2010) Biocompatible glass composite system—some physical-mechanical properties of the glass composite matrix system. Institute of Physics, Wrocław University of Technology, Wrocław, Optica Applicata
13. Niżankowski CZ (2002) Manufacturing sintered corundum abradants. Archives of Civil and Mechanical Engineering, Faculty of Mechanical Engineering Wrocław University of Technology, Wrocław
14. Staniewicz-Brudnik B, Szarska S, Gamrat K (2008) The influence of mechanochemical treatment of sintered submicrocrystalline corundum scaffolds on the structure of bioglass composites. J Superhard Mater 30(6):392–399. https://doi.org/10.3103/S1063457608060051
15. Young RA (1993) The Rietveld method. Oxford University Press
16. McCusker LB, Von Dreele RB, Cox DE et al (1999) Rietveld refinement guidelines. J Appl Crystallogr 32:36–50
17. Karolus M, Łągiewka E (2004) Crystallite size and lattice strain in nanocrystalline Ni-Mo alloys studied by Rietveld Refinement. J Alloys Compd 367:235–238
18. Karolus M (2006) Applications of rietveld refinement in Fe-B-Nb alloy structure studies. J Mater Process Technol 175:246–250
19. Wiliamson GK, Hall WH (1953) Acta Metall 1:22
20. Kosmulski M (2002) The pH-dependent surface charging and the points of zero charge. J Colloid Interface Sci 253:77–87. https://doi.org/10.1006/jcis.2002.8490
21. Coreño-Alonso J, Coreño-Alonso O, Merced M-R (2014) Apatite formation on alumina: the role of the initial adsorption of calcium and phosphate ions. Ceram Int 40(3):4909–4915